# $Ca^{2+}$-regulated structural changes in troponin

**Maia V. Vinogradova*, Deborah B. Stone*†, Galina G. Malanina*†, Christina Karatzaferi*, Roger Cooke*, Robert A. Mendelson*†‡, and Robert J. Fletterick*§**

*Department of Biochemistry and Biophysics, University of California, San Francisco, CA 94143-2240; and †Cardiovascular Research Institute, University of California, San Francisco, CA 94143-0130

Edited by Carolyn Cohen, Brandeis University, Waltham, MA, and approved February 18, 2005 (received for review November 30, 2004)

**Troponin senses $Ca^{2+}$ to regulate contraction in striated muscle. Structures of skeletal muscle troponin composed of TnC (the sensor), TnI (the regulator), and TnT (the link to the muscle thin filament) have been determined. The structure of troponin in the $Ca^{2+}$-activated state features a nearly twofold symmetrical assembly of TnI and TnT subunits penetrated asymmetrically by the dumbbell-shaped TnC subunit. Ca ions are thought to regulate contraction by controlling the presentation to and withdrawal of the TnI inhibitory segment from the thin filament. Here, we show that the rigid central helix of the sensor binds the inhibitory segment of TnI in the $Ca^{2+}$-activated state. Comparison of crystal structures of troponin in the $Ca^{2+}$-activated state at 3.0 Å resolution and in the $Ca^{2+}$-free state at 7.0 Å resolution shows that the long framework helices of TnI and TnT, presumed to be a $Ca^{2+}$-independent structural domain of troponin are unchanged. Loss of Ca ions causes the rigid central helix of the sensor to collapse and to release the inhibitory segment of TnI. The inhibitory segment of TnI changes conformation from an extended loop in the presence of $Ca^{2+}$ to a short $\alpha$-helix in its absence. We also show that Anapoe, a detergent molecule, increases the contractile force of muscle fibers and binds specifically, together with the TnI switch helix, in a hydrophobic pocket of TnC upon activation by Ca ions.**

Ca | muscle | regulation | structure

The sliding-filament theory of muscle contraction was proposed 50 years ago (for a historical survey, see ref. 1). During muscle contraction, the thick filament built of myosin molecules slides along the thin filament causing the muscle sarcomere to shorten. Troponin, tropomyosin, and actin constitute the thin filament (reviewed in ref. 2). Actin provides binding sites for the subfragment 1 region of myosin; tropomyosin affects the accessibility of these binding sites and troponin regulates the accessibility in a $Ca^{2+}$-dependent manner (3–6). Troponin consists of three subunits: TnT, TnI, and TnC (7). TnT binds to tropomyosin and anchors the troponin complex on the thin filament. In the presence of actin, TnI inhibits myosin ATPase cycle at low Ca levels. TnC responds to the rise in $Ca^{2+}$ concentration by removing the TnI inhibition (for review, see refs. 8 and 9).

Proteolysis by chymotrypsin divides TnT into two domains: TnT1 (amino acids 1–155 in skeletal troponin) and TnT2 (amino acids 156–262) (1). TnT1 interacts with tropomyosin; TnT2 is required for troponin assembly and also interacts with tropomyosin. The inhibitory properties of troponin are assigned to the inhibitory segment of TnI (amino acids 104–115) that can bind to actin in the absence of $Ca^{2+}$ (11). A second actin-binding site is at the C terminus of the TnI (amino acids 140–148) (12). The switch segment of TnI (amino acids 116–131) is the $Ca^{2+}$ transducer as it binds to the N terminus of $Ca^{2+}$-activated TnC (13). TnC is a $Ca^{2+}$-sensor that contains four EF-hands (14). A single $\alpha$-helix linker connects the N-terminal regulatory and C-terminal structural lobes into a dumbbell-shaped molecule (15–19). The regulatory metal binding sites 1 and 2 in the N-terminal domain prefer $Ca^{2+}$. Metal binding sites 3 and 4 in the C-terminal domain can be occupied by $Mg^{2+}$ in the relaxed state of muscle or by $Ca^{2+}$ during contractions (2).

Binding of $Ca^{2+}$ to the regulatory sites opens the EF-hands accompanied by the exposure of a hydrophobic cavity (17, 19). The TnI switch segment binds in this cavity (20) and is presumed to initiate other conformational changes in the thin filament facilitating myosin binding (21). One well known model for troponin regulation of myosin binding onto the thin filament is that binding of the TnI switch segment causes detachment of the TnI inhibitory segment from actin. Detachment would remove restraints on the position of tropomyosin on actin (6, 22). The released tropomyosin would move aside making the myosin binding sites more available and facilitating cooperative binding of myosin to the thin filament.

Because of its critical role in controlling the force of muscle contraction, TnC has been the subject of many drug-discovery projects (23–25). Enhancing the efficiency of $Ca^{2+}$ binding during muscle contraction is potentially important in cardiac diseases including heart failure. NMR and x-ray crystallography defined a locus in the regulatory lobe of TnC that interacts with both the TnI switch and one drug. Bepridil, a $Ca^{2+}$ sensitizer, was shown to bind to cardiac TnC in this locus and stimulate the opening of the N-terminal regulatory lobe (26, 27). Additional $Ca^{2+}$ ion sensitizing molecules were discovered in screens, but none are used clinically, and more effective and specific drugs are desirable.

Understanding the mechanism of muscle activation by $Ca^{2+}$ has been significantly slowed because of insufficient structural information for troponin. Crystallization of the troponin complex has been attempted many times during last 25 years, and recently, a high-resolution crystal structure of the cardiac troponin core domain in the $Ca^{2+}$-saturated state has been reported (28). However, the cardiac and skeletal isoforms of troponin are distinct structurally and physiologically (2, 29). Here, we describe the 3.0-Å crystal structure of skeletal muscle troponin complex in the $Ca^{2+}$-activated state and a 7.0-Å crystal structure in the $Ca^{2+}$-free state, and we show mechanistic features that are not found in the cardiac troponin structure.

## Methods

**Protein Purification and Complex Assembly.** The following recombinant constructs of chicken fast skeletal muscle troponin were used: TnC (amino acids 1–162) (the Ile-130 residue replaces Thr-130), Cys-less TnI (amino acids 1–182) (30), or TnI (amino acids 1–137), and TnT2 (amino acids 156–262). TnC and TnI subunits were expressed and purified as described (30). The expression and purification of TnT2 and complex assembly were as described in ref. 31, with modifications. Before crystallization, the ternary complex was isolated on a Superdex 75 gel-filtration column by using a protein buffer containing 50 mM Hepes (pH

This paper was submitted directly (Track II) to the PNAS office.

Data deposition: The atomic coordinates and structure factors have been deposited in the Protein Data Bank, www.pdb.org (PDB ID codes 1YTZ and 1YV0).

‡Deceased August 5, 2001.

§To whom correspondence should be addressed at: Department of Biochemistry and Biophysics, University of California, 600 16th Street, GHS-412E, San Francisco, CA 94143-2240. E-mail: flett@msg.ucsf.edu.

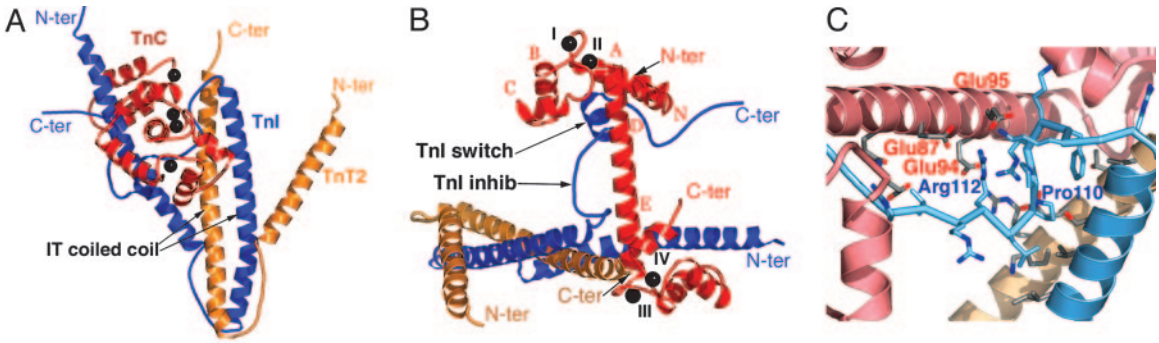


**Fig. 1.** Structure of skeletal troponin complex presented in two orientations. The troponin subunits are color-coded as follows: orange, TnT2; blue, TnI; and red, TnC. Black spheres indicate Ca. The termini of subunits are shown and color-coded as described above. (*A*) The nearly twofold symmetrical assembly of TnI and TnT2 subunits. The rotation angle that would create the best match between the subunits is ≈174°. (*B*) The TnC central helix is orientated perpendicular to the plane of TnI and TnT2. The capital-letter coding in red corresponds to the TnC helices in the N-terminal regulatory domain and for the central linker. The TnI inhibitory and switch segments are indicated. Roman numerals indicate the $Ca^{2+}$-binding sites. (*C*) Close-up view of the TnI inhibitory segment. The residues determining the position of the TnI inhibitory segment are shown as stick models. The colors in this image are faded to avoid confusion with the red and blue oxygens and nitrogens in the stick models.

7.5), 250 mM NaCl, 1 mM DTT, and either 2 mM $CaCl_2$ or 2 mM $MgCl_2$. The isolated complex was concentrated to 10–20 mg/ml.

**Crystallization.** The troponin complex in the presence of $Ca^{2+}$ was crystallized by using the sitting-drop vapor diffusion method and 0.4 M $NaH_2PO_4$/1.6 M $K_2HPO4$/200 mM NaCl in 0.1 M imidazole (pH 8.0) as the reservoir solution. Drops containing 2 $\mu$l of protein sample in the protein buffer and 2 $\mu$l of reservoir solution were equilibrated at 4°C for 5–10 days. Both $Ca(H_2PO_4)_2$ and $CaHPO_4$ are slightly soluble at 4°C; we estimated the free-$Ca^{2+}$ concentration to be >50 $\mu$M based on the dissociation constants at 0°C at pH 8.0. Before x-ray data collection, the crystals were transferred into a cryoprotecting solution containing 15% ethylene glycol in the reservoir and flash frozen in liquid nitrogen. These crystals diffracted to a resolution of 8.0 Å. The crystallization conditions were optimized by adding 0.5 $\mu$l of 10× stock solution of either Anapoe 305 or Anapoe 405 (compounds from Detergent Screen 2, Hampton Research, Riverside, CA) to the drop. Diffraction to a resolution of 3.0 Å was detected. Identical crystals grew in the presence of either Anapoe 305 or Anapoe 405. Both low- and high-resolution crystals exhibit the same tetragonal space group ($P4_32_12$) and identical cell dimensions ($a = b = 138.608$ Å, $c = 83.676$ Å).

Detergent was omitted for crystallization of the Ca-free troponin. The concentrated sample of troponin was purified and dialyzed without Ca and with 2 mM $MgCl_2$ and 1 mM EGTA before crystallization. Crystals appeared at room temperature with 1.4 M trisodium citrate dihydrate in 0.1 M Hepes (pH 7.5) in the reservoir. Before x-ray data collection, the crystals were transferred into a cryoprotecting solution containing 15% ethylene glycol in the reservoir and flash frozen in liquid nitrogen. The crystals diffracted to a resolution of 7.0 Å; the space group is the same as that for the crystals formed in the presence of $Ca^{2+}$ ($P4_32_12$), but the unit cell dimensions are different ($a = b = 134.662$ Å, $c = 102.072$ Å). Persistent trials to improve the resolution were unsuccessful.

**Data Collection, Model Building, and Refinement.** X-ray diffraction data were collected at the Advanced Light Source (Lawrence Berkeley National Laboratory, Berkeley, CA) beamline 8.3.1. ($\lambda = 1.1$ Å), processed by using DENZO and scaled by SCALEPACK (32). The structure of troponin in the $Ca^{2+}$-activated state was determined by molecular replacement (CNS; ref. 33) using atomic coordinates for the part of human cardiac troponin ternary complex (PDB ID code 1J1E). Various combinations of structural elements were tried as a search model, and the most successful combination contained TnT2 (residues 202–276) and TnC (residues 98–161). Electron-density maps were produced by using 2Fo-Fc coefficients and phases calculated from the initial model. The refinement was carried out by using CNS with manual rebuilding steps using QUANTA (Accelrys). The structure was checked and rebuilt by using annealed omit maps and the PROCHECK script from CCP4 (34). The crystallographic model is refined to $R_{cryst}$ and $R_{free}$ values of 28.2% and 33.3%, respectively (PDB ID code 1YTZ). It contains amino acid residues of TnC (2–161), TnI (3–143), and TnT2 (159–248), as well as 51 water molecules, four $Ca^{2+}$, and three molecules of Anapoe 305. The tails of Anapoe 305 molecules, which are 30 (—$CH_2$—$CH_2$—O—) groups long, were partially visible. In the model, they were built up to the length of four groups (—$CH_2$—$CH_2$—O—). There was no visible electron density for the 39 C-terminal amino acid residues (144–182) of TnI or the C-terminal residues of TnT2 (249–262).

The structure of troponin in the $Ca^{2+}$-free state was determined by molecular replacement (CNS; ref. 33) using the refined model of the troponin in the $Ca^{2+}$-activated state. The search model contained TnT2 (residues 159–248) and TnI (residues 3–101). The model building was done as described above. The crystallographic model is refined to $R_{cryst}$ and $R_{free}$ values of 35.8% and 35.9%, respectively (PDB ID code 1YV0). There is no unexplained electron density with contouring level at $\sigma = 1.0$ in the final map.

**Mechanical Measurements on Muscle Fibers.** Single permeable rabbit skeletal muscle fibers or strips of permeable rabbit cardiac tissue were mounted between a sensitive force transducer and a fast motor, and isometric tension was measured as a function of Ca concentration, as described (35, 36).

**Supporting Information.** For more information on refinement statistics and model building, see Table 1 and Figs. 6 and 7, which are published as supporting information on the PNAS web site.

## Results and Discussion

**Skeletal Troponin Complex.** We crystallized the troponin ternary complex derived from chicken fast skeletal muscle in the presence of $Ca^{2+}$ and determined the three-dimensional structure of the complex using x-ray crystallography (see *Methods*). Our proteins were made in *Escherichia coli*, and TnT is missing the TnT1 segment that leads to aggregation (31). The structure reveals a noncompact molecule (Fig. 1) that looks like two pairs

BIOPHYSICS

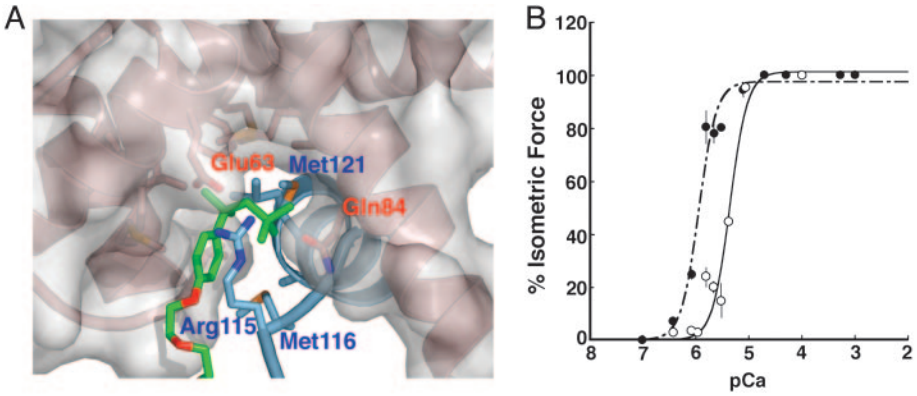


**Fig. 2.** Binding of Anapoe to the N-terminal domain of TnC. (*A*) The switch-binding pocket in TnC. The N-terminal domain of TnC is shown as a surface (gray) with a ribbon structure underneath. The TnI switch segment is shown as a ribbon. For color coding, see Fig. 1*C*. The residues involved in hydrophobic interactions between TnC and TnI are shown as stick models. The hydrophobic head of Anapoe is shown as sticks. The carbons of Anapoe are green; the oxygens are red. The colors in this image are faded to avoid confusion with the red and blue oxygens and nitrogens in the stick models. (*B*) A plot of isometric force versus $Ca^{2+}$; effect of addition of 1 mM Anapoe on $Ca^{2+}$ sensitivity of force production in rabbit psoas fibers. Data points are means ± estimated SDs for four to nine fibers for each data point at 10°C (pH 7). The continuous lines are drawn according to the parameters developed by fitting the data to the Hill equation, $P/P_0 = 1/(1 + 10^{(-nH(pCa50-pCa))})$, where pCa50 = 5.35 ± 0.04 and 5.94 ± 0.04 and $nH$ = 2.65 ± 0.52 and 2.63 ± 0.48 for the control (open circles) and the 1 mM Anapoe, respectively.

of chopsticks holding a dumbbell. The "W"-like assembly of TnI and TnT2 subunits that constitute the chopsticks shows nearly twofold symmetry (Fig. 1*A*). The long helices of the TnI (amino acids 58–102) and the TnT2 (amino acids 200–245) subunits interact with each other through a coiled coil (termed IT coiled coil here). The N-terminal helix of TnI (amino acids 8–48) and the IT coiled coil hold the C-terminal domain of TnC. The central linker of TnC forms a long $\alpha$-helix that runs almost perpendicular to the IT coiled coil and defines the extended dumbbell shape of the TnC subunit (Fig. 1*B*). Electron density, corresponding to $Ca^{2+}$ ($Mg^{2+}$ is not present in the crystals and the density is as expected for $Ca^{2+}$), is seen in the binding sites 1 and 2 of the N-terminal domain, as well as in binding sites 3 and 4 of the C-terminal domain of TnC. Helices B and C of the EF-hands in the regulatory domain are in the "open" conformation confirming the $Ca^{2+}$-activated state of troponin. The switch segment of TnI (amino acids 116–131) is bound to the regulatory domain of TnC between the helices of the opened EF-hands. The major regulator of actin-myosin association, the inhibitory segment of TnI (amino acids 104–115), visualized here, is an ordered loop that interacts with TnC (Fig. 1). This loop is stabilized by electrostatic interactions with TnC and hydrophobic interactions with TnI (Fig. 1*C*). The C-terminal 3 aa of the TnI inhibitory segment (amino acids 113–115) are stretched along the central helix of TnC, being uniquely ordered in this troponin complex but disordered in cardiac troponin (28) (Fig. 1*C*). Amino acids 132–143 of TnI after the switch segment also form a loop that binds to the N-terminal lobe of TnC. At the C terminus of TnI, ≈40 amino acid residues assumed to bind actin are disordered. This C-terminal part of TnI (amino acids ≈144–182) is also disordered in the solution structure of skeletal muscle troponin when $Ca^{2+}$ is bound (31).

The critical element regulating contraction, the TnI inhibitory segment, binds to the central helix of TnC only in $Ca^{2+}$ activated troponin. Because there are no intermolecular crystal contacts in this region, these mutually stabilized structural elements are likely to be found in the observed configuration *in vivo*.

**Intermolecular Interactions Within the Crystal of the Ca-Bound Troponin.** Few contacts are made between adjacent troponins in the crystal lattice reflecting the two-thirds solvent content. Neighboring molecule contacts likely have a minor influence on the structure. The N-terminal domain of TnC that is responsible for recognizing the regulatory $Ca^{2+}$ makes few van der Waals contacts to amino acid side chains from one symmetry-related molecule in the crystal. The conformation observed for TnC is as found in solution (31) and in other crystals of TnC (15–17). The structure of the N-terminal helix of TnT2, which contacts one partner in the crystal lattice may be different from the position found in solution (31), which would alter the nearly twofold symmetry (Fig. 1) relating TnT2 and TnI. This symmetry may mirror the proposed gene duplication in the evolution of TnT and TnI (37).

**$Ca^{2+}$ Binds More Effectively in the Presence of Anapoe.** Troponin saturated with $Ca^{2+}$ was crystallized in the presence of Anapoe (see *Methods* and Fig. 2*A*), a detergent used to optimize crystal quality for x-ray diffraction. Anapoe binds in the hydrophobic cleft formed upon $Ca^{2+}$-induced opening of the N-terminal domain of TnC. Binding of Anapoe is specific, supported by the hydrophobic side chains of eight amino acid residues comprising the pocket and the geometry of the cavity (Fig. 2*A*). Together with hydrophobic side chains of switch segment residues (Met-121, Leu-122, and Leu-125), the hydrophobic head of Anapoe 305 is located in the hydrophobic Met-rich environment of the pocket, whereas the polar residues of the switch segment (Asp-119 and Arg-123) and the polar tail of the detergent are located on the surface. Two other molecules of Anapoe bind on the surface of TnI and TnT2 helices far from the regulatory domain of TnC, and fewer and apparently weaker hydrophobic interactions are found at these surface sites. Together, these observations suggest that these molecules are not involved in the physiological effects of Anapoe (described below).

The crystals form with or without Anapoe, but diffraction without Anapoe is poor. Anapoe is likely to affect the dynamic stability of the troponin in the crystal in the $Ca^{2+}$-bound conformation. The detergent is unlikely to affect the conformation of troponin because the unit cell dimensions are not sensitive to Anapoe and because the troponin crystal structure is consistent with that determined with small angle neutron and x-ray scattering data obtained without Anapoe (31).

Note that the binding site discovered for Anapoe is where the drug bepridil binds to TnC (26). The effect of added Anapoe on the force of muscle contraction was measured by using skinned muscle fibers. In skeletal muscle, addition of the detergent increased the tension of a partially activated fiber in a dose-

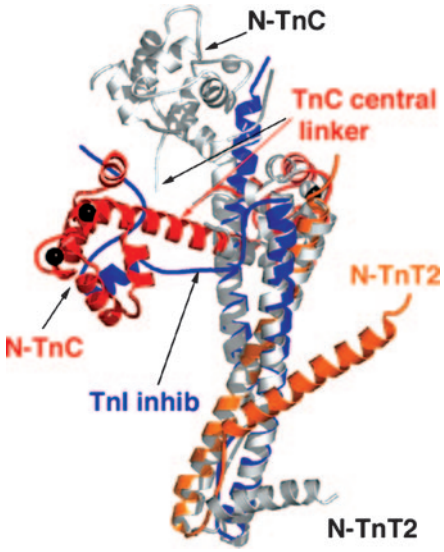


**Fig. 3.** Superposition of the structures of chicken skeletal muscle troponin and human cardiac troponin in the $Ca^{2+}$-saturated state. The structure of cardiac troponin (28) (PDB ID code 1J1D; chains A, B, and C) is shown in gray. Arrows indicate deviations.

dependent fashion with an apparent dissociation constant of 640 $\mu$M (data not shown). Addition of Anapoe to cardiac muscle also potentiated tension but to a lesser extent (apparent dissociation constant 4 mM, data not shown). Anapoe at a concentration of 1 mM enhanced the pCa by 0.5 ± 0.1, which corresponds to a 3- to 4-fold increase in sensitivity to $Ca^{2+}$ (Fig. 2*B*). Notably, the detergent does not alter the tension of nonactivated or fully activated fibers. The $Ca^{2+}$ cooperativity, as measured by the apparent Hill coefficient, was unchanged. Anapoe either facilitates binding of $Ca^{2+}$ to the regulatory sites or potentiates the effect of bound $Ca^{2+}$. These data, and the position for Anapoe at the TnI switch should prompt efforts to find a physiological agent that functions like bepridil or Anapoe.

**Structural Differences Between Skeletal and Cardiac Isoforms of Troponin.** Conformational differences between the skeletal and cardiac isoforms of troponin have been observed at ≈30 Å resolution in the solution structures of binary and ternary complexes derived from small-angle neutron-scattering data (30, 38) and in the NMR solution structures of TnC (19, 39). $Ca^{2+}$-binding site 1 in cardiac TnC is inactive because of isoform amino acid replacements (40). The N-terminal domain of cardiac TnC does not open as much as in skeletal TnC in the presence of $Ca^{2+}$ (39). At the N terminus of the TnI subunit, the cardiac isoform has an extension of 33 aa. Functionally, the troponins differ; $Ca^{2+}$ affects cardiac troponin less (29).

Comparison of the structures of cardiac and skeletal muscle troponins showed that the overall organization of the subunits in these complexes is similar (see Fig. 3). However, the following four prominent features do not correspond: the location of the TnC $Ca^{2+}$ regulatory domain; the conformation of the central linker; the structure of the TnI inhibitory segment, which is ordered and visible only in the skeletal muscle isoform; and the position and conformation of the N terminus of TnT2. As expected from published data, the switch segment binding pockets differ, with the skeletal muscle complex being more open. The TnC $Ca^{2+}$ regulatory domain is positioned in space by the central helix of TnC, which is rigid in skeletal TnC, whereas it is melted in cardiac TnC. The different conformations of the central helix in the two troponins place their TnC N-terminal regulatory domains in locations that are 28 Å apart. Likely resulting from the ordered central helix, the TnI inhibitory region is very well ordered in skeletal troponin, whereas it is flexible and not visible in the cardiac troponin crystal structure.

What accounts for the differences and do they alter the regulatory mechanisms of the two troponins? The crystal packing of skeletal troponin is less tight than in cardiac troponin (66% vs. 52% of solvent content in the skeletal and cardiac troponin crystals, respectively) and the crystal contacts are less extensive in skeletal troponin crystal. The position of the TnC N-terminal domain in cardiac troponin (PDB ID codes 1J1E and 1J1D) is possibly determined by the interactions with neighbors in the crystal and the weakly ordered central helix.

The rigid central helix might be required for skeletal TnC to bind TnI and to relay structural changes to tropomyosin. Consistent with this suggestion, an intact central helix linker was shown to be important for orienting the structural and regulatory domains of TnC and maintaining its function in skeletal troponin (41–43). According to neutron-scattering data, skeletal TnC is extended in the $Ca^{2+}$-activated ternary complex and in the TnC-TnI binary complex (30, 31, 44); these data agree with the intact central helix conformation seen here. The interaction of the inhibitory region of TnI with the central linker of TnC was detected in $Ca^{2+}$-activated skeletal troponin in crosslinking studies (45).

The flexibility of the TnC central linker has been assessed for cardiac troponin. Flexibility decreases significantly in the presence of TnI inhibitory peptide or intact cardiac TnI as detected by NMR analysis (46, 47). We speculate that the central helix of cardiac TnC is disordered in the crystal structure because of packing constraints. In solution or *in vivo*, interactions with the missing cardiac-specific N-terminal extension of TnI, and with inhibitory segment of TnI, could assist stabilization of the central helix.

The binding pocket for the switch segment in the N-terminal domain of TnC differs in skeletal and in cardiac troponin. In a two-step process, $Ca^{2+}$ binds forming the pocket then the switch inserts into the pocket. Binding of the switch segment promotes the opening of EF-hands in the N-terminal domain of cardiac TnC which are in the closed conformation even after $Ca^{2+}$ has bound (19, 39). Still, even with the switch segment bound, the binding pocket is less open in the cardiac troponin complex (28) compared with that in the skeletal troponin complex. The switch segment binds in the $Ca^{2+}$-opened pocket of skeletal TnC through multiple hydrophobic contacts. In addition, the switch segment is registered by electrostatic interactions between TnC residues Glu-63 and Gln-84 and TnI residue Arg-115 on the outside of the pocket (Fig. 2*A*). The conserved replacement of the polar residue to hydrophobic in the cardiac TnC (Gln-84 to Cys-84) reorients the side chains of the TnI residue Ile-149 and TnC residue Cys-84 toward the pocket, enhancing the hydrophobic interactions within the cardiac switch-binding pocket and defining its tighter and more compact architecture.

Binding of bepridil, a $Ca^{2+}$-sensitizer, to cardiac TnC was shown to enlarge the switch-binding pocket (27). From data that are not shown here, Anapoe increases the tension of cardiac fibers, suggesting that this compound is likely to bind to cardiac TnC and has the same effect on the cardiac TnC switch-binding pocket as bepridil.

**Skeletal Troponin Complex in the $Ca^{2+}$-Free State.** To understand the conformational changes in troponin upon $Ca^{2+}$ activation that lead to the regulation of muscle contraction, we crystallized the chicken skeletal muscle troponin in the $Ca^{2+}$-free state. The 7-Å resolution x-ray diffraction data allowed us to visualize the positions of $\alpha$-helices and, therefore, the relative positions of structural domains in troponin in the $Ca^{2+}$-free state (Fig. 4*A*). The central linker of TnC loses its helical conformation and is disordered, which causes the $Ca^{2+}$ regulatory N-terminal do-

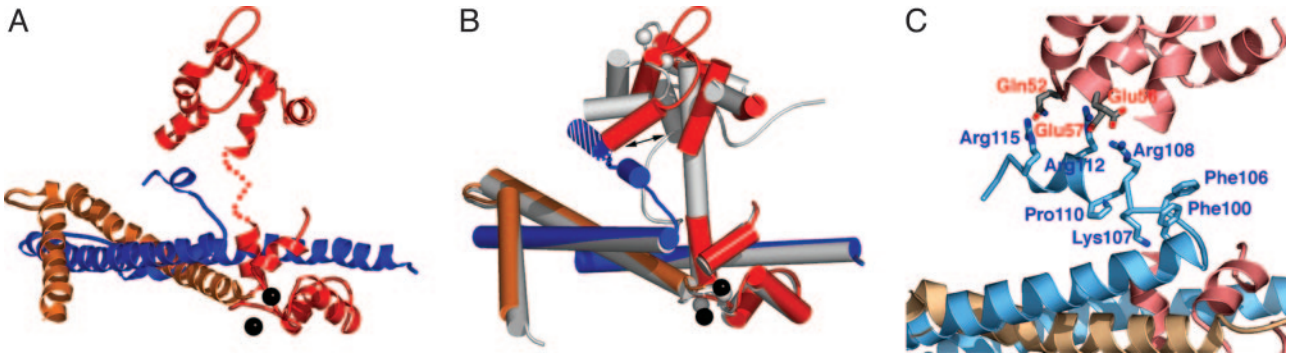


**Fig. 4.** Structure of skeletal troponin in the $Ca^{2+}$-free state. (*A*) Positions of $\alpha$-helices determined in the $Ca^{2+}$-free troponin. The loops in TnC are simulated. The disordered central linker in TnC is shown as a red dotted line. (*B*) Superposition of the structures of skeletal muscle troponin in the $Ca^{2+}$-free and $Ca^{2+}$-activated states. The structures are shown as cylinder models. The structure of troponin in $Ca^{2+}$-activated state is shown in gray. The hypothetical position of the TnI switch segment in the $Ca^{2+}$-free state structure is shown by the stripped (blue and white) cylinder. (*C*) Interactions possibly stabilizing the TnI inhibitory segment in the $Ca^{2+}$-free state. Residues modeled to be involved in these interactions are shown as sticks. For color coding, see the legend to Fig. 1. The colors in this image are faded to avoid confusion with the red and blue oxygens and nitrogens in the stick models.

main of TnC to rotate 38° relative to its position in the $Ca^{2+}$-activated state (Fig. 4*B*). The TnI switch segment (gray helix, arrow, Fig. 4*B*) dissociates from the TnC hydrophobic cleft in the $Ca^{2+}$-activated structure, which is now closed (Fig. 4*B*). New electron density appears in the $Ca^{2+}$-free troponin corresponding to an $\alpha$-helix of 9–10 aa. This strong electron density is observed between the N-terminal domain of TnC and the IT coiled coil. Modeling a polyAla helical peptide into this density improved the refinement statistics, although no side chains were resolved.

When modeling further, we took into account the secondary structure predictions and various sequence registers and modified the geometric conformations of the side chains. Only one model showed a noticeable improvement of the refinement statistics (see *Methods* and Fig. 7). Based on this model, the newly observed density belongs to the inhibitory segment of TnI. The inhibitory segment residues 110–115 are proposed to form a short $\alpha$-helix initiated by Pro-110. A distorted helical turn (residues 107–109) and a well ordered loop (residues 104–106) precede this helix. The first N-terminal residues of the switch segment (residues 116–118), immediately after the inhibitory region, were also fit into the density. The electron density map allows no unoccupied volume for an additional helix. Therefore, we assume that the switch helix was destabilized under the $Ca^{2+}$-free crystallization conditions. Apparently, upon closure of the hydrophobic pocket on TnC, the hydrophobic residues of the TnI switch segment did not find helix-stabilizing contacts in the crystals.

The new conformation and configuration of the inhibitory segment is now stabilized by electrostatic interactions with surface residues of the TnC N-terminal domain (Fig. 4*C*). Possibly, TnI residue Arg-108 and residues Glu-56 and Glu-57 of TnC form ionic bonds reflected in the connected electron density. The conformation of the loop connecting the N terminus of the TnI "inhibitory helix" and the IT coiled coil are presumably supported by the hydrophobic cluster interactions formed by Phe-100, Phe-106, and the long aliphatic side chains of Lys-107 and Arg-108. These interactions define a sharp turn of this loop and make it very well ordered.

The inhibitory segment has changed its conformation from an extended loop in the presence of $Ca^{2+}$ to a short $\alpha$-helix in the absence of $Ca^{2+}$. Secondary structure predictions are compatible with the inhibitory segment being helical. A loop-to-helix transition would be possible with the release of constraints from the disordered central helix and the expelled TnI switch segment. The ≈8 Å movement of the TnI inhibitory segment residues and the residues of the following hypothetical switch segment (Fig. 4*B*) agrees with measurements of proximity between TnC and TnI and between TnI and actin using photocrosslinking and FRET (48–50).

**Mechanism of Troponin Regulation.** Assuming that our identification of the helical inhibitory segment in the new position is correct, we propose a model for troponin activation and relaxation (Fig. 5).

During muscle activation, $Ca^{2+}$ binding would induce opening of the hydrophobic pocket in the N-lobe of TnC and the TnI switch segment would bind there. Opening of the N-terminal domain of TnC and repositioning of the TnI switch segment restores the helical conformation of the central linker of TnC and removes the TnI inhibitory segment from actin by dragging and stretching it along the central helix. The central helix of TnC and the TnI inhibitory segment loop are mutually stabilized.

Upon closing of the pocket in the $Ca^{2+}$-free state of troponin in relaxed muscle, the switch segment is expelled and the TnC central linker loses its helical conformation. With a loss of stabilization by the TnC central helix, the TnI inhibitory segment is released and assumes a soft $\alpha$-helical conformation. This conformation of the inhibitory segment is supported by electrostatic interactions with surface residues of the TnC regulatory domain. Then the inhibitory segment is free to interact with actin. Thus the $Ca^{2+}$ sensor is coordinated through loop-and-helix transitions triggered by binding and freeing the switch. The suggested role (2) of the rest of the troponin core (N-terminal helices of TnI and TnT2 and the IT coiled coil) is to orient and position the troponin complex on the actin–tropomyosin filament. This idea is supported by the fact that these parts did not

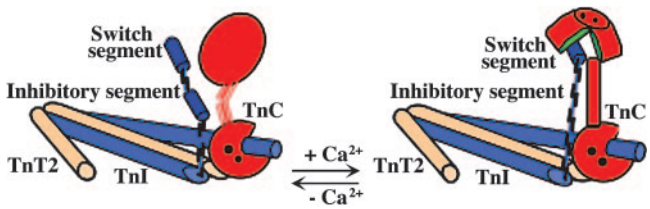


**Fig. 5.** Cartoon representation of the conformational changes occurring in troponin during muscle contraction. For color coding, see the legend to Fig. 1. Ca ions are shown as black circles. The hydrophobic pocket opened in the N-terminal lobe of TnC is colored in green. The switch segment and the inhibitory segment of TnI are indicated.

change their relative positions in the structures of $Ca^{2+}$-activated and $Ca^{2+}$-free states of troponin.

The steric blocking mechanism (21, 51, 52) proposes further that removal of the TnI inhibitory segment from actin affects the position of the bound tropomyosin, which becomes less restrained and able to move on the actin surface. The increased flexibility of tropomyosin increases the accessibility of the myosin binding sites and favors myosin binding to the actin filament. Existing data lead to the following three-state model of the thin filament (22, 54, 55): Blocked state (minus Ca), Closed state (plus Ca), and Open state (plus Ca and bound myosin). The exact correspondence between our structures and these three states is not clear, but it would appear to be reasonable that our Ca-free structure represents the Blocked conformation, and the Ca-bound structure represents the Closed conformation.

The most detailed model for the role of TnI in the $Ca^{2+}$-activated regulation of striated-muscle contraction is that of Luo *et al.* (53). According to this model, the TnI inhibitory segment is removed from actin by the interaction of the triggering regulatory switch segment with the TnC N-terminal domain hydrophobic cleft. Our work provides a structural basis for this model by defining the conformational changes in the TnI inhibitory segment.

We thank Dr. Carlos Ramos for providing the DNA construct of the TnI (residues 1–137) and Drs. Paul Curmi and Elena Sablin for helpful discussion. This work was supported by National Institutes of Health Program Project Grant P01AR42895 and Grants R01AR45659 and R01GM067830.

1. Huxley, H. E. (2004) *Eur. J. Biochem.* **271,** 1403–1415.
2. Gordon, A. M., Homsher, E. & Regnier, M. (2000) *Physiol. Rev.* **80,** 853–924.
3. Ebashi, S., Endo, M. & Otsuki, I. (1969) *Q. Rev. Biophys.* **2,** 351–384.
4. Parry, D. A. & Squire, J. M. (1973) *J. Mol. Biol.* **75,** 33–55.
5. Lehman, W., Craig, R. & Vibert, P. (1994) *Nature* **368,** 65–67.
6. Xu, C., Craig, R., Tobacman, L., Horowitz, R. & Lehman, W. (1999) *Biophys. J.* **77,** 985–992.
7. Greaser, M. L. & Gergely, J. (1971) *J. Biol. Chem.* **246,** 4226–4233.
8. Perry, S. V. (1998) *J. Muscle Res. Cell Motil.* **19,** 575–602.
9. Perry, S. V. (1999) *Mol. Cell. Biochem.* **190,** 9–32.
10. Mak, A. S. & Smillie, L. B. (1981) *J. Mol. Biol.* **149,** 541–550.
11. Van Eyk, J. E., Thomas, L. T., Tripet, B., Wiesner, R. J., Pearlstone, J. R., Farah, C. S., Reinach, F. C. & Hodges, R. S. (1997) *J. Biol. Chem.* **272,** 10529–10537.
12. Tripet, B., VanEyk, J. E. & Hodges, R. S. (1997) *J. Mol. Biol.* **271,** 728–750.
13. Pearlstone, J. R., Sykes, B. D. & Smillie, L. B. (1997) *Biochemistry* **36,** 7601–7606.
14. Nakayama, S. & Kretsinger, R. H. (1994) *Annu. Rev. Biophys. Biomol. Struct.* **23,** 473–507.
15. Satyshur, K. A., Rao, S. T., Pyzalska, D., Drendel, W., Greaser, M. & Sundaralingam, M. (1988) *J. Biol. Chem.* **263,** 1628–1647.
16. Herzberg, O. & James, M. N. (1988) *J. Mol. Biol.* **203,** 761–779.
17. Houdusse, A., Love, M. L., Dominguez, R., Grabarek, Z. & Cohen, C. (1997) *Structure (London)* **5,** 1695–1711.
18. Vassylyev, D. G., Takeda, S., Wakatsuki, S., Maeda, K. & Maeda, Y. (1998) *Proc. Natl. Acad. Sci. USA* **95,** 4847–4852.
19. Slupsky, C. M. & Sykes, B. D. (1995) *Biochemistry* **34,** 15953–15964.
20. Mercier, P., Ferguson, R. E., Irving, M., Corrie, J. E., Trentham, D. R. & Sykes, B. D. (2003) *Biochemistry* **42,** 4333–4348.
21. Potter, J. D. & Gergely, J. (1974) *Biochemistry* **13,** 2697–2703.
22. McKillop, D. F. & Geeves, M. A. (1993) *Biophys. J.* **65,** 693–701.
23. Pan, B. S. & Johnson, R. G., Jr. (1996) *J. Biol. Chem.* **271,** 817–823.
24. MacLachlan, L. K., Reid, D. G., Mitchell, R. C., Salter, C. J. & Smith, S. J. (1990) *J. Biol. Chem.* **265,** 9764–9770.
25. Sorsa, T., Heikkinen, S., Abbott, M. B., Abusamhadneh, E., Laakso, T., Tilgmann, C., Serimaa, R., Annila, A., Rosevear, P. R., Drakenberg, T., *et al.* (2001) *J. Biol. Chem.* **276,** 9337–9343.
26. Wang, X., Li, M. X. & Sykes, B. D. (2002) *J. Biol. Chem.* **277,** 31124–31133.
27. Li, Y., Love, M. L., Putkey, J. A. & Cohen, C. (2000) *Proc. Natl. Acad. Sci. USA* **97,** 5140–5145.
28. Takeda, S., Yamashita, A., Maeda, K. & Maeda, Y. (2003) *Nature* **424,** 35–41.
29. Maytum, R., Westerdorf, B., Jaquet, K. & Geeves, M. A. (2003) *J. Biol. Chem.* **278,** 6696–6701.
30. Stone, D. B., Timmins, P., Schneider, D. K., Krylova, I., Ramos, C. H. I., Reinach, F. C. & Mendelson, R. A. (1998) *J. Mol. Biol.* **281,** 689–704.
31. King, W. A., Stone, D. B., Timmins, P. A., Narayanan, T., von Brasch, A. A. M., Mendelson, R. A. & Curmi, P. M. G. (2005) *J. Mol. Biol.* **345,** 797–815.
32. Otwinowski, Z. M., W. (1997) *Methods Enzymol.* **276,** 307–326.
33. Brunger, A. T. *et al.* (1998) *Acta Crystallogr. D* **54,** 905–921.
34. Collaborative Computational Project N (1994) *Acta Crystallogr. D* **50,** 760–763.
35. Karatzaferi, C., Myburgh, K. H., Chinn, M. K., Franks-Skiba, K. & Cooke, R. (2003) *Am. J. Physiol.* **284,** C816–C825.
36. Martyn, D. A., Gordon, A. M. (1988) *J. Muscle Res. Cell Motil.* **9,** 428–445.
37. Barton, P. J., Mullen, A. J., Cullen, M. E., Dhoot, G. K., Simon-Chazottes, D. & Guenet, J. L. (2000) *Mamm. Genome* **11,** 926–929.
38. Heller, W. T., Abusamhadneh, E., Finley, N., Rosevear, P. R. & Trewhella, J. (2002) *Biochemistry* **41,** 15654–15663.
39. Sia, S. K., Li, M. X., Spyracopoulos, L., Gagne, S. M., Liu, W., Putkey, J. A. & Sykes, B. D. (1997) *J. Biol. Chem.* **272,** 18216–18221.
40. van Eerd, J. P. & Takahshi, K. (1976) *Biochemistry* **15,** 1171–1180.
41. Sheng, Z. L., Francois, J. M., Hitchcock-DeGregori, S. E. & Potter, J. D. (1991) *J. Biol. Chem.* **266,** 5711–5715.
42. Ramakrishnan, S. & Hitchcock-DeGregori, S. E. (1995) *Biochemistry* **34,** 16789–16796.
43. Ngai, S. M. & Hodges, R. S. (2001) *J. Cell. Biochem.* **83,** 33–46.
44. Olah, G. A., Rokop, S. E., Wang, C. L., Blechner, S. L. & Trewhella, J. (1994) *Biochemistry* **33,** 8233–8239.
45. Kobayashi, T., Tao, T., Gergely, J. & Collins, J. H. (1994) *J. Biol. Chem.* **269,** 5725–5729.
46. Abbott, M. B., Gaponenko, V., Abusamhadneh, E., Finley, N., Li, G., Dvoretsky, A., Rance, M., Solaro, R. J. & Rosevear, P. R. (2000) *J. Biol. Chem.* **275,** 20610–20617.
47. Gaponenko, V., Abusamhadneh, E., Abbott, M. B., Finley, N., Gasmi-Seabrook, G., Solaro, R. J., Rance, M. & Rosevear, P. R. (1999) *J. Biol. Chem.* **274,** 16681–16684.
48. Luo, Y., Leszyk, J., Li, B., Gergely, J. & Tao, T. (2000) *Biochemistry* **39,** 15306–15315.
49. Kobayashi, T., Kobayashi, M., Gryczynski, Z., Lakowicz, J. R. & Collins, J. H. (2000) *Biochemistry* **39,** 86–91.
50. Li, Z., Gergely, J. & Tao, T. (2001) *Biophys. J.* **81,** 321–333.
51. Vibert, P., Craig, R. & Lehman, W. (1997) *J. Mol. Biol.* **266,** 8–14.
52. Lehman, W., Rosol, M., Tobacman, L. S. & Craig, R. (2001) *J. Mol. Biol.* **307,** 739–744.
53. Luo, Y., Leszyk, J., Li, B., Li, Z., Gergely, J. & Tao, T. (2002) *J. Mol. Biol.* **316,** 429–434.
54. Craig, R. & Lehman, W. (2001) *J. Mol. Biol.* **311,** 1027–1036.
55. Hai, H., Sano, K., Maeda, K., Maeda, Y. & Miki, M. (2002) *J. Biochem.* **131,** 407–418.